Vertical Structure in Atmospheric Fog and Haze and Its Effects on Visible and Infrared Extinction

R. G. PINNICK, D. L. HOIHJELLE, G. FERNANDEZ, E. B. STENMARK, J. D. LINDBERG AND G. B. HOIDALE

U.S. Army Atmospheric Sciences Laboratory, White Sands Missile Range, NM 88002

S. G. JENNINGS

Department of Pure and Applied Physics, University of Manchester Institute of Science and Technology, Manchester, England

(Manuscript received 14 February 1978, in final form 5 June 1978)

ABSTRACT

Vertical structure of the size distribution and number concentration of particulates in atmospheric fog and haze near Grafenwöhr, West Germany, were measured with a balloonborne light-scattering aerosol counter for periods spanning parts of eight days in February 1976. For haze (~5 km visibility) conditions, little vertical variation is seen; but for low visibility (<1 km) fog conditions, significant vertical increases in concentration of droplets with radii larger than 4 μm are seen over the first 150 m altitude. For haze, the particle size distribution is approximated by a log-normal with geometric mean radius $r_g \approx 0.2$ μm and geometric standard deviation $\sigma_g \approx 1.9$. For fog, a bimodal distribution is found with a relative maximum for the larger particle mode at radii of 4 to 6 μm and corresponding values $r_g \approx 5$ μm and $\sigma_g \approx 1.6$; the smaller particle mode has values of $r_g \approx 0.3$ μm to $r_g \approx 0.6$ μm and $\sigma_g \approx 1.8$ to $\sigma_g \approx 2.5$. Liquid water content values for haze and fog range from 10^{-4} to 0.45 g m^{-3}. Extinction calculated from the particle size distributions shows an approximate $1/\lambda$ wavelength dependence for haze conditions, but nearly neutral (wavelength independent) extinction for heavy fog. A correlation exists between calculated particulate extinction and calculated liquid water content, independent of particle size distribution, for the fogs and hazes studied.

1. Introduction

The presence of atmospheric fog and haze is important to radiative transfer in the atmosphere. For example, fog and haze particles degrade the performance of electro-optical systems and affect the earth's climate. Quantitative estimates of these effects generally require knowledge of the vertical variation of fog and haze particle size distributions. Near-surface size distribution measurements have been made by impaction techniques (Garland, 1971; Krasikov and Chikirova, 1956; Kumai, 1973; Low, 1975; May, 1961; Barteneva and Polyakova, 1965), by collection of particles on spiderwebs (Arnulf *et al.*, 1957), by a laser hologram camera (Kunkel, 1971) and by light-scattering single-particle counters (Eldridge, 1961; Laktionov, 1967). However, measurement of the vertical structure of fog and haze particle size distributions are difficult to make and are consequently rather sparce with some exceptions (Pilié *et al.*, 1975; Goodman, 1977). Both Pilié *et al.* and Goodman used impaction techniques to measure droplet spectra to 150–200 m altitudes. Impaction measurements involve laborious microscope measurement of droplets or droplet replicas which restrict their usefulness, as only a relatively small number of distributions can realistically be determined. Furthermore, corrections must be applied to obtain true droplet size and collection efficiencies must be known to obtain relative particle concentrations.

In this paper we present measurements of the size distributions of fog and haze particles made with a tethered, balloonborne, light-scattering particle counter, with emphasis on their effect on radiation for visible through middle-infrared wavelengths. The primary advantage of using a light-scattering counter over an impactor technique is that the measurement is done *in situ* in real time with minimal disturbance to the particles during measurement. Measurement of vertical structure of atmospheric fog and haze under relatively stable conditions is possible with this technique because a statistically significant size distribution measurement can be completed in approximately ½ min, permitting an upleg and downleg profile to 200 m altitude to be completed in 15–30 min.

The purpose of this paper is to present the vertical structure of fog and haze that occurred in a wintertime continental environment in Germany, as measured with

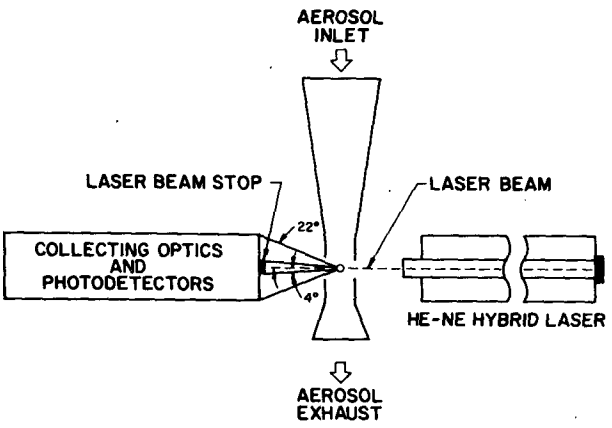

FIG. 1. Schematic of the Particle Measurement Systems CSAS light-scattering aerosol counter optical system.

a light-scattering counter, in the form of particle number, area and volume distributions, and in the form of extinction and liquid water content values calculated from the measured distributions. An additional purpose is to investigate the spectral dependence of extinction, and to examine correlations between extinction and liquid water content. Measurements reported here were made during February 1976 near Grafenwöhr, a town located 100 km north of Nürnberg near the eastern border of West Germany. The local terrain consists of rolling hills and is partially forested; some of the land is tilled for farming.

Because the light-scattering counter technique offers only an indirect measure of particle size, and because the particular instrument we used is heretofore untested, we first give in Section 2 a discussion of its calibration. The balloon experiment data collection procedures are described in Section 3. In Section 4 typical haze and fog profiles are presented, together with discussion of their significance regarding propagation of radiation. Finally, in Section 5 the relation between extinction and liquid water content of fog and haze is investigated.

2. Aerosol detector description and calibration

The aerosol detector used for the measurements reported here is the Knollenberg (after R. G. Knollenberg, the developer) Classical Scattering Aerosol Spectrometer (CSAS) manufactured by Particle Measurement Systems, Inc. (PMS), Boulder, Colorado. A schematic of the optical system of this instrument is shown in Fig. 1. The device works on the principle that as aerosol particles flow through an illuminated volume, light scattered into a particular (near forward

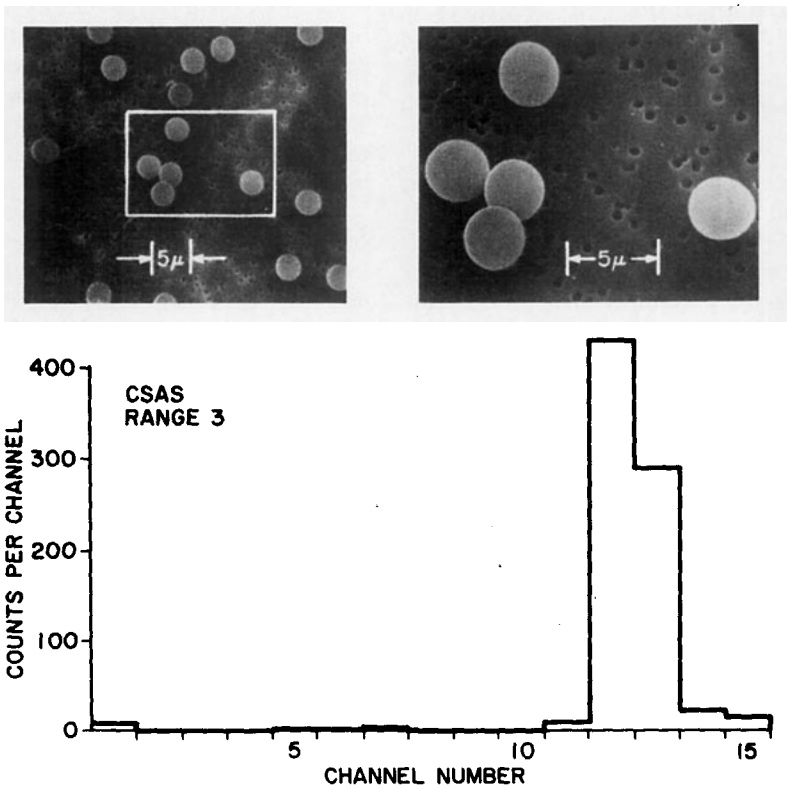

FIG. 2. A typical CSAS pulse-height spectrum for monodisperse aerosol. This particular spectrum is for solid particles of nigrosin dye with mean radius 1.78 μm; a scanning electron microscope micrograph of several of these particles collected onto a Nuclepore filter is also shown. The black circles are holes in the filter substrate.

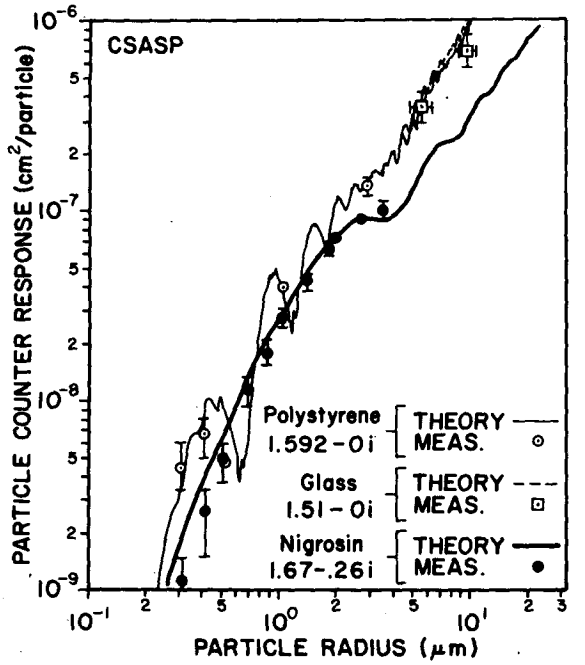

FIG. 3. Comparison of Particle Measurement Systems CSAS particle counter measured response (circles and squares) and calculated response using Mie scattering theory (smooth curves) for single spherical particles versus particle size. Measured values have been normalized for the best fit to the theoretical values for polystyrene latex particles with refractive index 1.592–0*i*. The theoretical curve for glass beads with refractive index 1.51–0*i* extends only to about 4 μm radius.

scattering) solid angle by a single particle is measured photoelectrically and is used to determine particle size by electronically classifying response pulses according to their magnitude. The response signal can be related to particle size by a calibration supplied by the manufacturer. One problem with using the manufacturer's calibration is that it does not consider the refractive index of the particle measured. Particles of the same size but of different composition give significantly different response pulses; therefore, we deem it necessary to address the question of the instrument calibration in some detail.

In order to make a definitive measure of the CSAS response characteristics, monodisperse aerosols with known sizes and indexes of refraction are needed. We generated uniform spherical particles of nigrosin dye (index $=1.67-0.26i$, $\lambda=6328$ Å) with a technique described earlier (Pinnick *et al.*, 1973) and measured particle sizes using electron microscopy. We also generated uniform particles of polystyrene latex (index $=1.592-0i$, $\lambda=5893$ Å) available from Dow Chemical, by atomizing the hydrosol samples (diluted with distilled water). Measurement of uniform aerosol with the CSAS results in a peak in the pulse height spectrum; the position of the peak is a measure of the response of the instrument to aerosol of that size and refractive index. A typical spectrum for monodisperse aerosol of nigrosin dye is shown in Fig. 2, together with a scanning electron microscope micrograph of several of these particles collected onto a Nuclepore filter. The response of the CSAS to solid particles of nigrosin dye and polystyrene latex are shown in Fig. 3. Typical errors in response measurements are also shown. The errors in measurement of particle radii are less than the size of the dots marking the measurements. The squares in Fig. 3 denote response measurements for nearly monodisperse crown glass beads (index $=1.51-0i$, $\lambda=5893$ Å) available from Particle Information Services, Inc., Grants Pass, Oregon. The standard deviation in particle size of these beads is shown by the horizontal "error" bars, and the standard deviation in response pulses by the vertical "error" bars.

The measured response is expressed in cross section per particle normalized to the computer-calculated Mie theoretical results (solid-line curves) for best fit to the theoretical response for polystyrene latex aerosols. The theoretical response curves take into account the wavelength of the He–Ne laser light source (6328 Å) and the geometry of the light-collecting optics as in Fig. 1. The light-collecting solid angle has axial symmetry with respect to the direction of the laser light source. Light scattered into a cone subtending angles 4–22° from the direction of forward scattering is sensed by the instrument. The measured response and the response calculated with Mie scattering theory are in general agreement within errors of measurement. Therefore a measure of confidence can be placed in response curves calculated for spherical particles with indexes of refraction different from those studied here.

Response calculations for the CSAS instrument for water particles with complex refractive index 1.33–0*i*, for ammonium sulfate particles with index 1.50–0*i*, and for absorbing atmospheric dust particles with indexes 1.50–0.01*i* and 1.50–0.05*i*, are shown in Fig. 4. The results show a strong dependence of the response on the particle refractive index and a multivalued response for particles with diameters $\gtrsim 0.8$ μm. The calculated response is obviously sensitive to the particle refractive index for indexes in the range of those of atmospheric aerosols. The seriousness of the multivaluedness is reduced if only a small number of particle size channels are utilized in the multichannel analyzer. Of course, the size resolution of the instrument is reduced accordingly.

The manufacturer's pulse height discriminator level settings for our particular CSAS instrument are indicated by tick marks in Fig. 4. There are 15 particle size channels for each "range" of the instrument. Pulse height channels 1, 5, 10 and 15 are labeled between the appropriate tick marks. Changing range is merely an adjustment of an amplifier gain and thus has the effect of shifting the range of sensitivity.

Even if the particulates measured are all of the same known composition, there are—on some ranges—

discriminator levels set in regions of multivalued response. Nevertheless, size distribution information for a polydispersion of spherical particles can be determined by reducing the number of channels to avoid these regions.

To infer particle size distributions from the fog and haze measurements reported here, we have assumed the particles are water droplets (with refractive index 1.33–0*i*) and have grouped the particle size channels to avoid regions of multivalued response. This channel grouping for water particles is indicated by the heavy tick marks in Fig. 4. Specific channel size limits for the different ranges of the instrument can be determined from this figure by noting at what radii on the water response curve the appropriate heavy tick marks correspond. The light and heavy tick marks together indicate the manufacturer advertised channel discriminator levels. The channels are redefined with less size resolution than the response curve dictates because in practice statistical spectra broadening effects result in some channel cross sensitivity. Specifically, even a perfectly monodisperse aerosol results in a range of pulse heights, and identical particles are not counted entirely in one particle size channel. Therefore, use of discriminator levels set near regions of multivalued response has been avoided. The calibration scheme reduces the number of channels for each range from 15 to 7. The redefined channels are not of equal width.

Our assumption that the particles are homogeneous water droplets is obviously safe for the case of fog. For dry haze particles this assumption can lead to significant errors in the calibration, even if the particles are spherical. However, for the haze conditions during which we have made measurements that are reported here, the relative humidity as measured by sling psycrometer was nearly 100%. Theoretical predictions of the refractive index of aerosol as a function of relative humidity by Hänel (1971) suggest that the deviations of particle indexes from those of water (at visible wavelengths) are small for relative humidities greater than 95%, in terms of the resulting differences in the instrument response to these particles. Thus the haze particles are approximated by homogeneous water droplets.

The counting efficiency of the instrument for particles with radii >15 μm is less than 100%, since non-isokinetic sampling causes some of these larger particles to be lost in the instrument intake before a measurement is made. Air containing aerosol sampled with this instrument flows at 340 ℓ min^{-1} through a conical intake tube 45 cm long with a maximum diameter of 10 cm and a minimum diameter of 3.3 cm. The fraction of particles lost in this tube with radii of 15 μm is estimated to be less than 7%. The aerosol counter was pointed into the prevailing wind during measurement periods, although the effect of wind (which was generally <3 m s^{-1}) is not believed to be significant.

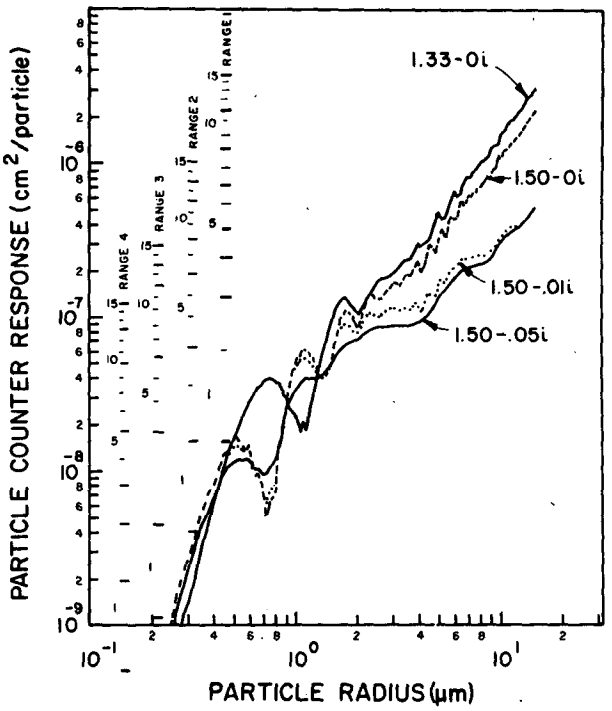

FIG. 4. Mie theory response calculations for the Particle Measurement Systems CSAS particle counter for water particles with refractive index 1.33–0*i*, ammonium sulfate with approximate index 1.50–0*i*, and atmospheric dust with indexes 1.5–0.01*i* and 1.50–0.05*i*. The tick marks indicate the pulse-height discriminator level settings as set by the manufacturer for the detector. Channels 1, 5 and 15 are labeled between the appropriate tick marks for the different range settings of the instrument. The heavy tick marks indicate the pulse-height discriminator level settings used in grouping channels together to avoid regions of multivalued response under the assumption that all particles are water.

A comment is in order here concerning the coincidence scheme utilized in the instrument to reject or accept particles depending on whether or not they pass through the "sample volume." Only a small fraction ($\sim$0.003%) of particles flowing through the instrument are actually measured because of the relatively small sample volume. The purpose of the coincidence scheme is to reject particles which are not within a sufficiently uniform (to within 10% according to PMS) part of the laser beam by opto-electronically discriminating against out-of-focus particles. There is evidence to suggest that this scheme results in a sample volume that is somewhat dependent on particle sizes. In other words, the instrument flow rate may be different for different size channels. However, simultaneous measurements made on uniform aerosols in our laboratory with both the CSAS and a particle counter of a special design developed by Rosen (1968) suggest this effect is less than 30%, at least for particles with radii <1 μm. A more complete account of the aerosol detector calibration problem is in preparation.

3. Data collection procedures

The basic goal of the experiment was to obtain information on vertical profiles of particle size distribution during atmospheric fog and haze conditions. To accomplish this, the CSAS particle counter together with temperature and visible radiation flux sensors were incorporated into a single payload weighing approximately 9 kg and carried aloft to a maximum altitude of 250 m by a 1500 ft^3 tethered balloon. Digitized data were sent via a wire link to a data acquisition unit on the ground; this link also furnished power to the payload. A photograph of the system is shown in Fig. 5.

This experiment was done as part of a much larger field exercise, and as a result considerable constraint on operating schedules was imposed. For example, there was a problem caused by the presence of a nearby radar station, so that data could only be collected when the radar was not in operation. In addition, the balloon experiment could not be operated at night because it was not equipped with lights which were required to meet local aircraft hazard warning regulations. Choice of actual operating conditions (ascent and descent rates, and altitude intervals) were determined by a compromise between the need for long counting intervals to produce statistically meaningful aerosol size distribution results, the desire for short counting intervals to obtain reasonable vertical spacial resolution, and the need to complete the ascent/descent in a relatively short time interval because of continually changing atmospheric conditions.

A choice was also made in the field controlling the CSAS counter size range (see Fig. 4). Under the assumption of spherical water droplets the following size ranges were used: range 1, 0.5–16 μm radius; range 2, 0.37–8 μm radius; range 3, 0.29–4 μm radius; range 4, 0.24–1.6 μm radius. Since the range setting could not be changed remotely, measurements made during an upleg and downleg traverse were necessarily made for a single range setting, optimized to cover the most important range of particle size for the widely different fog and haze size distributions encountered.

The usual operational procedure for a particular balloon traverse was to sample intermittently (with the CSAS positioned at a fixed altitude and set on 30–60 s accumulation times) at 30 m altitude intervals during the upleg portion, and to sample continuously (with the CSAS continuously moving and set on 20–30 s accumulation times) during the downleg portion. Since the size distribution measurements made during upleg and downleg portions of each traverse compared well, and since more vertical resolution was obtained during the downleg portion, we concentrate only on the latter. Thus, particle size distribution measurements reported here have been obtained by integrating over 8–12 m altitude intervals (depending on the CSAS accumulation time), as the payload descent rate was about 0.4 m s^{-1}. The altitude identified with a particular size distribution is the lower limit of the corresponding altitude

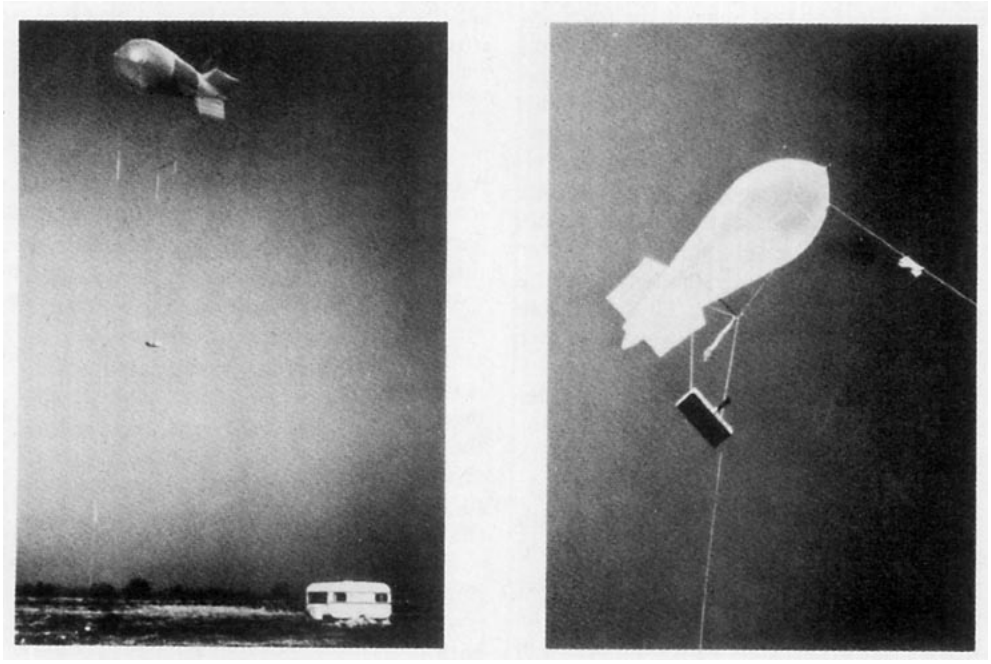

FIG. 5. Photographs of the balloonborne aerosol detector system used for fog and haze measurements near Grafenwöhr, West Germany. The detector (a light-scattering aerosol counter model CSAS manufactured by Particle Measurement Systems) is suspended ~15 m below the 1500 ft^3 tethered balloon and is rigged so that the detector intake points into the prevailing wind. Temperature and radiation flux sensors are incorporated into the payload.

interval. During heavy fog conditions it was not possible to achieve altitudes greater than 150 m, as copious amounts of water and rime condensed onto the balloon and tether line, reducing the balloon lift capability.

4. Haze and fog results

Four profiles of haze and fog, typical of 19 profiles measured during eight days in February 1976 near Grafenwöhr, are presented in Figs. 6–8. These show the vertical structure in terms of particle number ($dN/d\log r$), cross sectional ($dS/d\log r$) and volume ($dV/d\log r$) distributions. Some of the particle counter measurements (solid lines) have been fitted with log-normal size distributions (dashed curves) for the purpose of estimating the effects of extending and smoothing the measured size distributions. The reason for showing the area and volume distributions is that for limiting regimes of particle size the extinction cross section is nearly proportional to either the integrated cross-sectional area (for particles large compared to the wavelength) or volume (for particles small compared

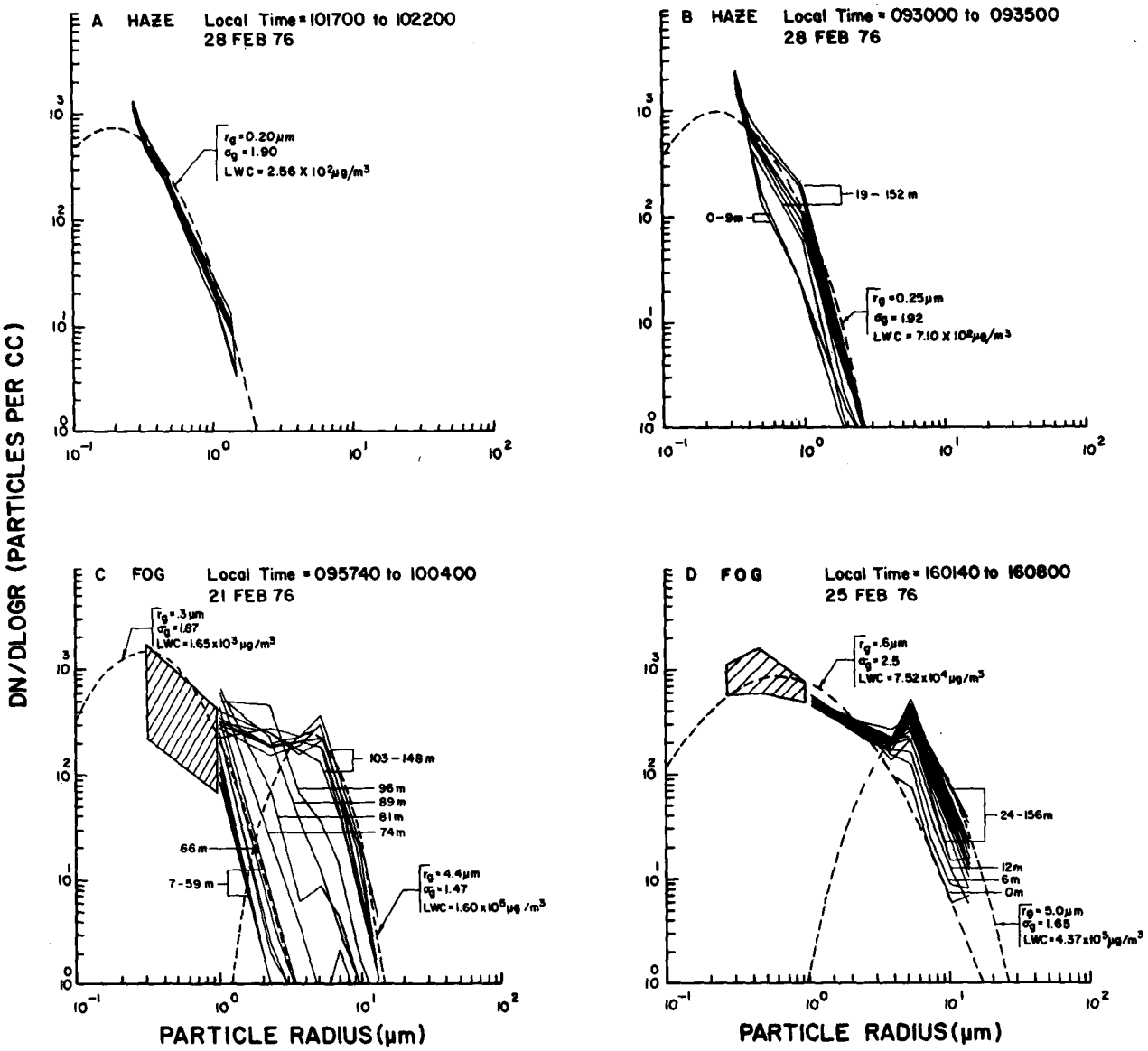

FIG. 6. Particulate size distribution measurements made near Grafenwöhr, West Germany, with a tethered balloonborne aerosol counter for several haze and fog conditions. Each size distribution is for a particular altitude or altitude range as indicated. Measurements at particular altitudes (121 m in Fig. 6a, 95 m in Fig. 6b, 59 and 126 m in Fig. 6c, and ground level and 135 m in Fig. 6d) have been fitted with log-normal size distributions (dashed curves) for the purpose of estimating the effects of extrapolating the measured distributions. Values of geometric mean radius r_g, geometric standard deviation σ_g and liquid water content LWC are shown with the corresponding log-normal curves. The date, local time (hours, minutes, seconds) and time interval for the measurements are given.

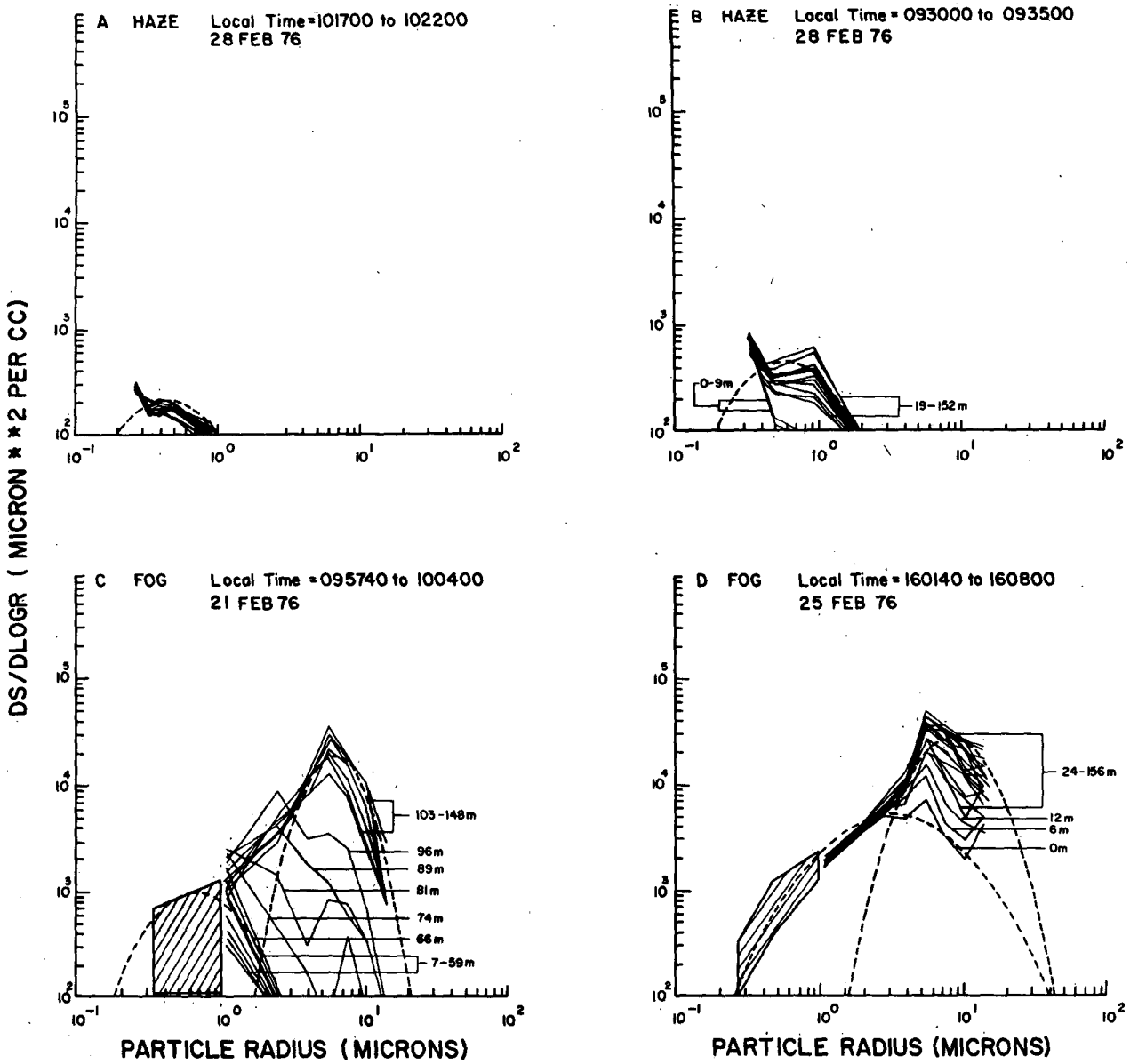

FIG. 7. As in Fig. 6 except for particle area (cross-sectional) distribution.

to the wavelength, as will be discussed in a following section). These distributions can therefore be used to infer the range of particle sizes that contribute most to extinction. Generally the values for $dN/d\log r < 10$ cm^{-3} are based on fewer than 10 particle counts per size channel and thus have large statistical errors.

Corresponding profiles of the liquid water content (LWC) and extinction coefficients calculated from the measured and fitted distributions at 0.55, 4 and 10 μm wavelengths are shown in Fig. 9. Note that the abscissa scales are different for the different parts of Fig. 9. The LWC and extinction for the fitted size distributions are calculated only for one or two altitudes for each profile in Fig. 9. The Mie single scatter extinction coefficients were calculated from

$$\beta_{\text{ext}} = \int_0^\infty \pi r^2 Q_{\text{ext}}(m,x) \frac{dN(r)}{dr} dr, \qquad (1)$$

where $N(r)$ is the particle concentration for particles with radius $\geq r$ and Q_{ext} is the Mie efficiency factor defined as the ratio of single particle extinction to the particle geometric cross section. The particle complex refractive index is m and the size parameter $x = 2\pi r/\lambda$ is the ratio of the particle circumference to the wavelength. The refractive indexes of water taken from Hale and Querry (1973) at each wavelength were used in

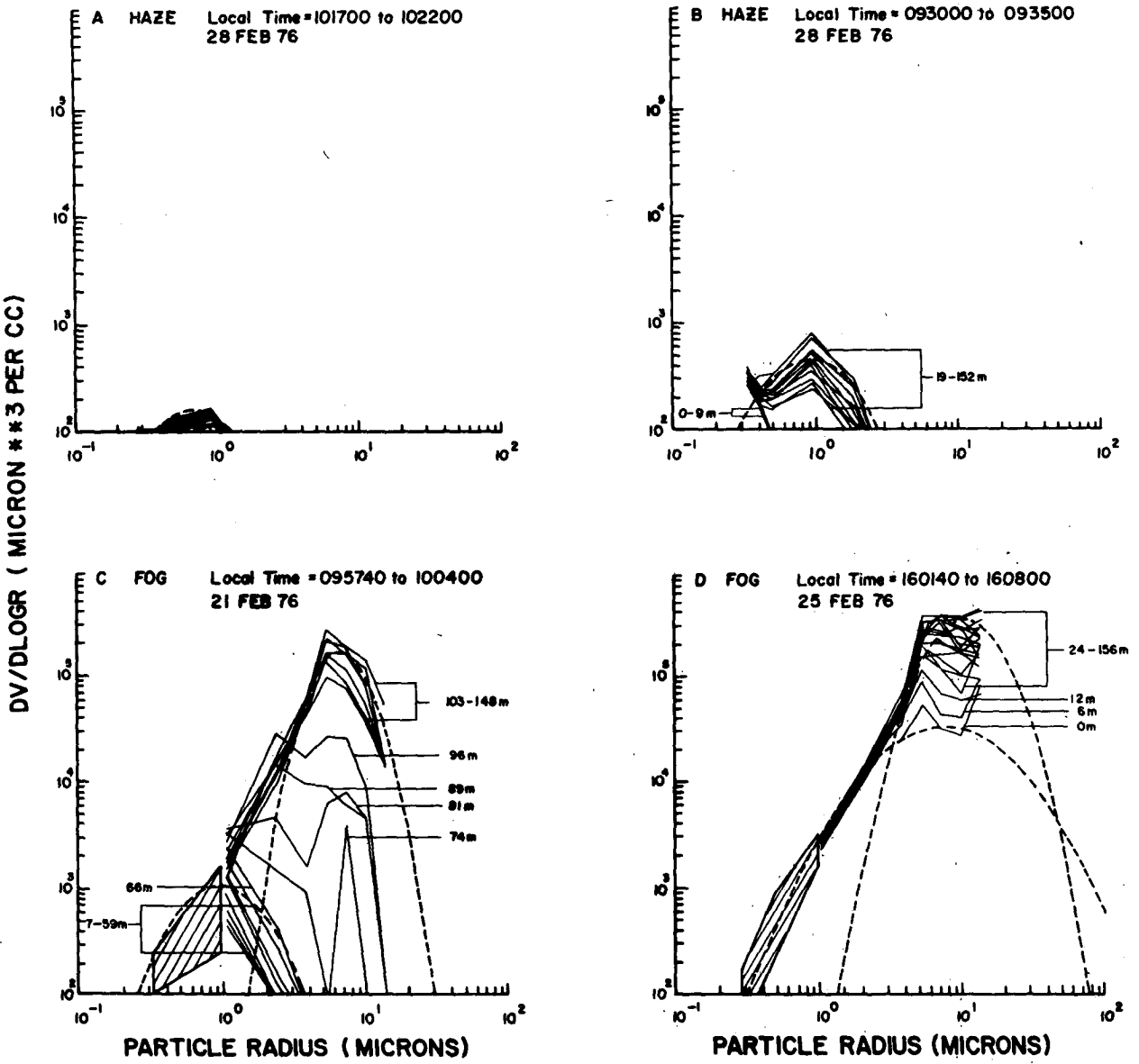

FIG. 8. As in Fig. 6 except for particle volume distribution.

Mie calculations of the extinction coefficients on the basis of the size distributions at a given altitude.

As stated above, log-normal size distributions were fitted to measured size distributions at particular altitudes in Figs. 6–8 so as to estimate the effect of extrapolating the measured distributions to both smaller and larger sizes. A qualification should be made concerning the comparison of Mie extinction and LWC results calculated from the measurements with results calculated from the log-normal size distributions. Namely, the calculations based on the measured distributions are for a distinct number of size channels (7) and the number of particles (cm^{-3} μm^{-1}) is assumed uniform in each channel. In other words, calculations for the measured distributions are for a particle size distribution histogram. The fitted log-normal distributions differ from the measured distributions in two ways: 1) the fitted distribution is an extrapolation of the measured distribution over both smaller and larger particle sizes and 2) the fitted distribution smooths the measured distribution so that the number of particles (cm^{-3} μm^{-1}) is not constant within each size channel. The effect of smoothing the measured distribution tends to cancel the effect of extending it. In fact, the combined effect of smoothing and extrapolating the measured distributions generally leads to smaller values

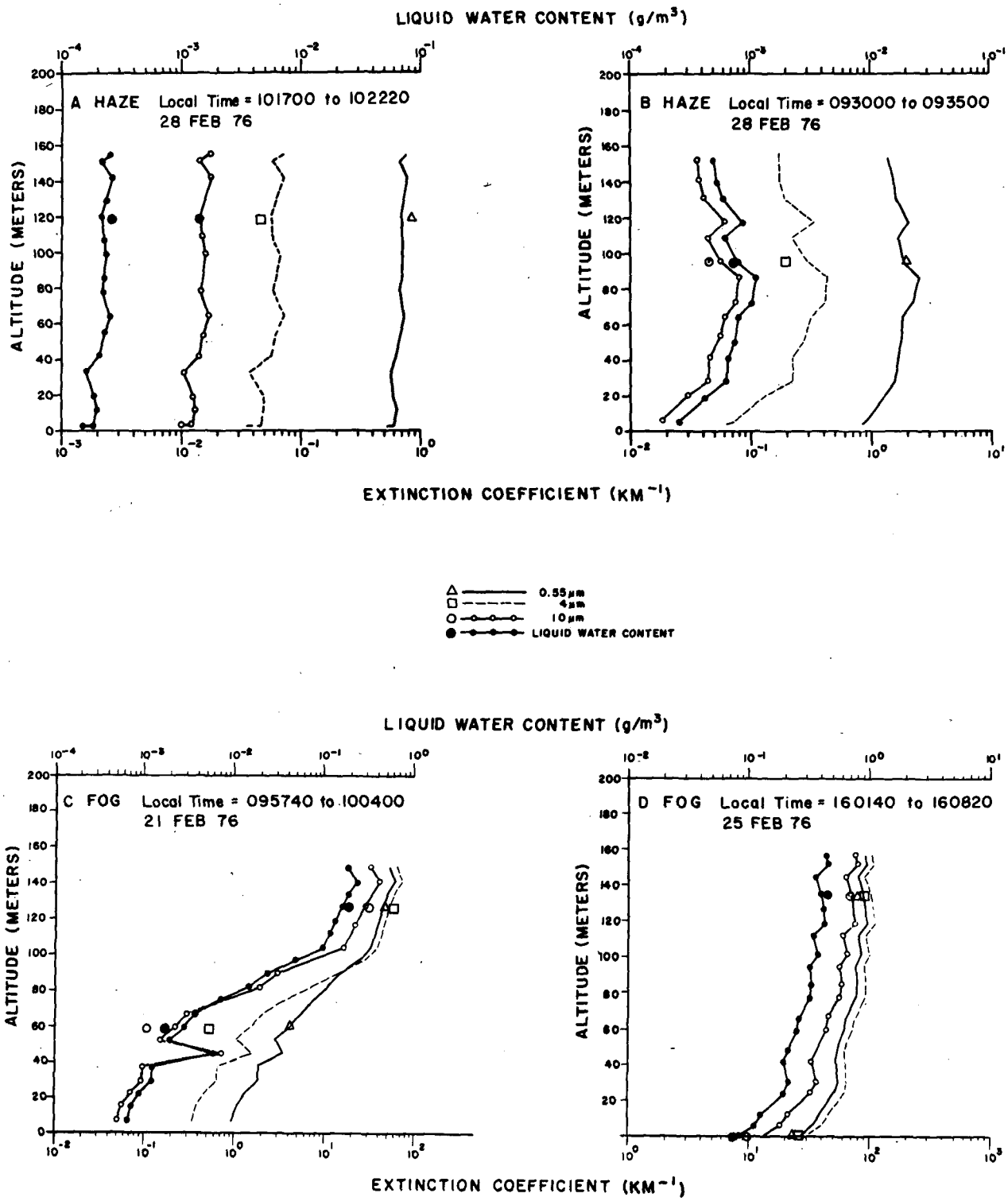

FIG. 9. Profiles of particulate extinction and water content calculated from particle size distribution and concentration measurements shown in Fig. 6. The solid-dot curve indicates the liquid water content and the solid-dashed and open-dot curves indicate the extinction at 0.55, 4 and 10 μm wavelengths. Calculations of the extinction and LWC for particular log-normal distributions fitted to measured distributions (Figs. 6–8) are shown at the corresponding altitudes, and are denoted by triangle, square, open-circle, and solid-circle symbols for extinction at 0.55, 4 and 10 μm, and liquid water content. The date, local time (hours, minutes, seconds) and time interval for the measurements are given.

of calculated extinction and LWC as compared to values calculated directly from the measured distribution.

The 28 February data in Figs. 6a–8a for a light haze condition show little vertical structure in size distribution. The 16 measured size distributions have been used to calculate extinction coefficients and LWC at corresponding altitudes in Fig. 9a. Calculations of extinction and LWC (Fig. 9a) for a log-normal size distribution fitted to the measured size distribution at 121 m altitude show that effects of extrapolating the distribution are small. The temperature lapse rate was stable for this traverse, the temperature changing from 1.1°C at ground level to −0.1°C at 155 m.

The particulate size distribution (Figs. 6b–8b) and extinction (Fig. 9b) for a haze condition an hour earlier on 28 February shows more vertical variation. A visual estimate of 2 km horizontal visibility was made during this trasverse. Using Koschmieder's formula to relate visibility to extinction for a threshold contrast ratio of 2% yields a value of 1.96 km^{-1} extinction for this haze condition, comparing favorably with extinction at 0.55 μm (Fig. 9b) calculated from the measured size distributions.

The fog data in Fig. 6c show large increases in concentration of 4–16 μm radius particles with altitude and Figs. 7c, 8c and 9c show the effects of these increases. The cross-hatched areas indicate the altitude variation in measurements made during traverses before and after the traverse in question, with the instrument set so as to sense smaller particles. Assuming that temporal changes are relatively small during these series of traverses (a period of about 2 h for all traverses was involved here), the cross-hatched areas show the approximate shape of the envelope of the distribution for smaller particles. Generally, the concentration of these smaller particles increased with altitude. The temperature lapse rate for this traverse is again stable with a ground temperature of −3.3°C. The calculated extinction coefficients and LWC in Fig. 9c vary by 2 to 3 orders of magnitude over this 150 m traverse. Comparison of results from the measured and fitted log-normal size distributions suggest that effects of smoothing and extrapolating the measured distribution are significant (as much as a factor 2 in extinction at 10 μm, but nearly zero at 0.55 μm) for altitudes less than about 70 m. At higher altitudes, the effects of smoothing and extrapolating the size distributions would appear to be relatively small, since at 126 m the differences in extinction and LWC are less than 5%. For the largest particle size channel (centered at 14 μm radius) the number of counts for this traverse is not statistically significant. In fact, the point to which six number, area and volume size distribution curves (at altitudes 111–148 m) converge in Figs. 6c–8c correspond to only 1 particle count for each curve. Nevertheless, the trend in the size distributions for the next two smaller size channels (centered at 12 and 9 μm) strongly suggest the measured fog distributions can be adequately extrapolated to larger particle sizes with the log-normal. Further, the shape of the distribution for the larger particle sizes is in good agreement with the preceding upleg measurements made about 15 min earlier. We point out here that the measured distribution at 126 m altitude was actually fitted by a sum of three log-normal distributions (two of which are shown here) to better accommodate the measurements in the 1–4 μm radius interval.

It is noteworthy that during this traverse a visual siting of the balloon payload was lost at 148 m altitude. Integrating the 0.55 μm extinction coefficient profile over the first 148 m of this traverse, we find an optical depth of 3.02, a value 23% lower than expected from the Koschmieder relation. Considering the uncertainty in making a visibility estimate and in applying the Koschmieder relation to relate visibility to optical depth, we judge this to be good agreement.

The heavy fog data in Fig. 9d show increasing extinction coefficient with altitude, again caused by the increased concentration of 4 to 16 μm radius particles shown in Figs. 6d–8d. The 21 size distribution curves in Fig. 6d were used to calculate extinction coefficients and LWC presented in Fig. 9d. In contrast to the 21 February fog, vertical increases in extinction and LWC are only about a factor 2–4. Again the cross-hatched areas in Figs. 6d–8d show the shape of distributions for submicrometer particles for a balloon traverse made 30 min after the traverse in question. This traverse is similar to six traverses made during stable fog conditions 25–26 February 1976 in Grafenwöhr. Ground wind speed for each of these traverses was generally <2 m s^{-1}, suggesting the fog was radiation type rather than advection type. Here it is evident that the log-normal extrapolation to particle sizes larger than those measured may be significantly in error, particularly in calculations of LWC (Fig. 8d) and extinction at 10 μm, for which a third mode of larger particles may contribute significantly, even though their relative number may be small. However, although a third mode of larger fog particles cannot be ruled out, a bimodal nature of the distributions is in agreement with measurements of wintertime radiation fogs in England by Garland (1971), Garland *et al.* (1973) and Roach *et al.* (1976), and some radiation fog measurements by Krasikov and Chikirova (1956) near Leningrad. The extinction coefficient is neutral (wavelength independent) within a factor of about 2, the extinction at 4 μm being slightly greater than that at 0.55 and 10 μm. Errors due to size distribution extrapolation and smoothing, assuming no mode of particles with radii greater than 16 μm is important, are small. The nearly neutral extinction for low visibility conditions has been found by Patterson (1977) for soil-derived aerosols as well, suggesting that a broad range of low (<1 km) visibility atmospheric conditions results in neutral extinction from visible wavelengths through the middle-infrared (0.5–10 μm).

Each of the four haze and fog profiles presented here is for a downleg portion of a balloon traverse. The corresponding upleg values of extinction and liquid water content are generally within 50% of the downleg values, so that temporal changes encountered are usually small compared to the vertical variations. These four profiles are typical of the 19 profiles taken during eight days at Grafenwöhr. For haze conditions, little vertical variation in the size distribution is observed; but for fog conditions, there are significant increases in the concentration of droplets with radii $\gtrsim 4$ μm. Measurements of the downward visible radiation flux made with a photodetector attached to the balloon package show that for each of the traverses the flux change with altitude was $<10\%$. This suggests that the fog or haze depths were somewhat greater than the maximum altitudes attained.

The trend toward increasing concentration of larger droplets with increasing altitude is in agreement with measurements of advection fogs over San Francisco by Goodman (1977), although in direct contradiction to previous measurements of continental fogs, notably

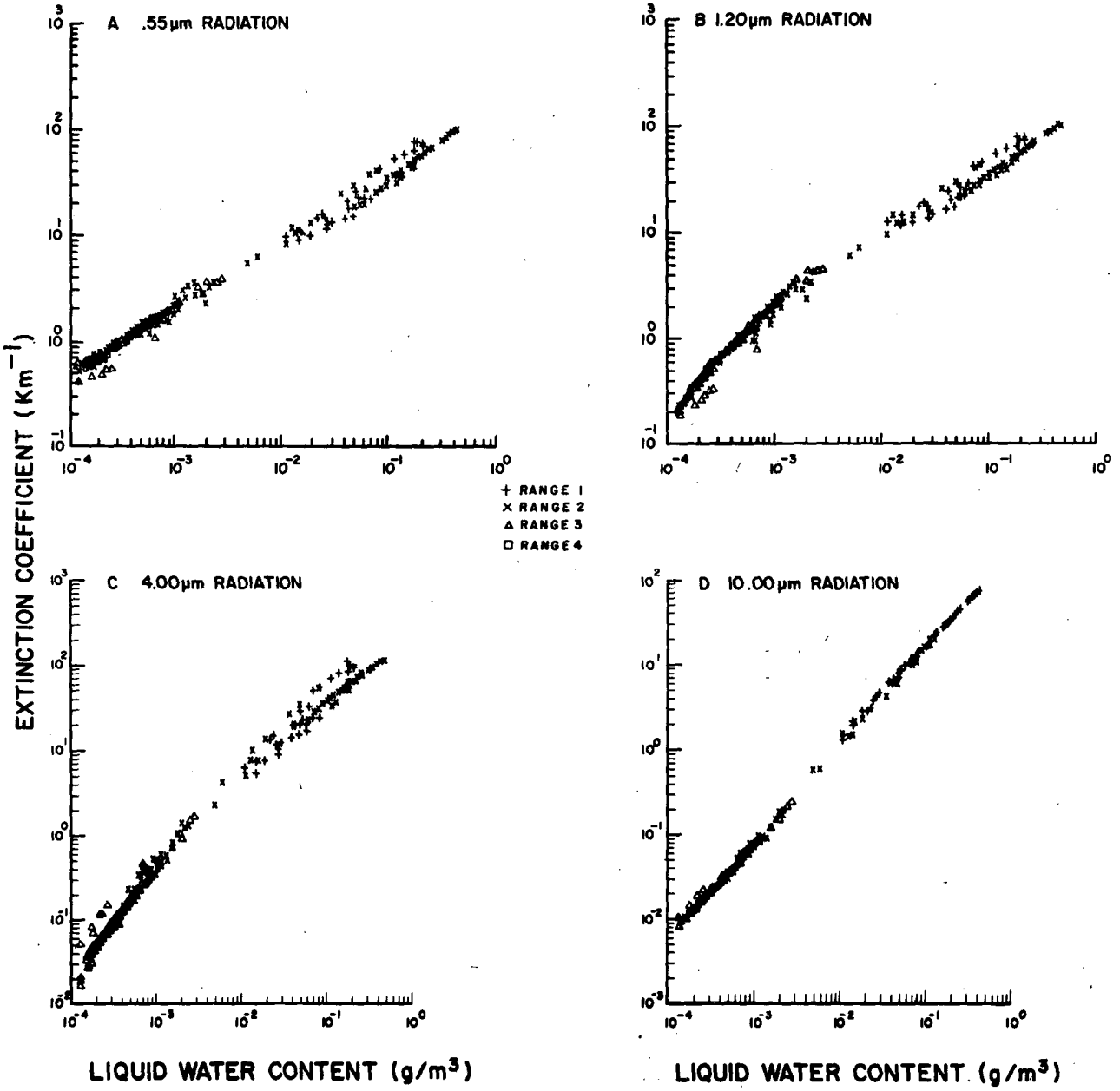

FIG. 10. Values of Mie theory calculated particulate extinction at 0.55, 1.2, 4 and 10 μm wavelengths versus liquid water content for a variety of particle size distributions of atmospheric fog and haze measured during February 1976 near Grafenwöhr, West Germany.

those of Pilié *et al.* (1975) for fogs in the Chemung River Valley near Elmira, NY. In view of the paucity of definitive measurements of the vertical structure of fog and haze, similar measurements at different geographical locations and under different meteorological conditions are clearly warranted.

5. Extinction and liquid water content of fog and haze

To investigate the correlation of particulate extinction and liquid water content evident in Fig. 9, these data, along with data from the remaining 15 balloon traverses made in Grafenwöhr, appear in Fig. 10. Plotted are values of the Mie calculated extinction for 0.55, 1.2, 4 and 10 μm wavelengths versus the liquid water content. Each point corresponds to a size distribution measurement made with the aerosol counter.

These results show approximate relationships between extinction and liquid water content, for 289 measured distributions of fog and haze with liquid water content values ranging over four orders of magnitude. Such relationships have been noted before at visible wavelengths by Eldridge (1966, 1971), Barteneva and Polyakova (1965) and Kumai (1973). Recently, Chýlek (1978) has shown that in fact a linear relationship should exist between extinction and LWC, independent of particle size distribution, but only for a wavelength determined by the radii of the largest particles present in the polydispersion of droplets. This is a result of the efficiency factor for extinction Q_{ext} being nearly proportional to size parameter x, which leads to extinction being proportional to LWC, providing droplets have size parameters less than a maximum value x_m. The maximum size parameter, $x_m \approx 7$, but it depends slightly on refractive index and hence on wavelength. If we choose a wavelength of 10 μm, then $x_m = 8$ (Chýlek, 1978) and according to the Chýlek approximation we should find a linear relation between extinction and LWC for polydispersions of droplets having radii $r \leqslant 12$ μm. Most of our haze and fog distributions satisfy this condition and, as verified in Fig. 10, there does exist a nearly linear relation between extinction at 10 μm and LWC. Even for heavy fog the presence of larger droplets ($r > 12$ μm), insofar as they do not dominate the smaller ones, does not destroy the linear size distribution independent relation. However, the fact that there are approximate relationships between extinction and LWC for shorter wavelengths (*viz.*, 0.55, 1.2 and 4 μm) for heavy fog (for which particles with $x > 7$ dominate extinction) is probably a result of the common form of the measured fog distributions (see, for e.g., Fig. 6d), since for arbitrary distributions and wavelengths there is no reason to expect a unique relationship between extinction and LWC.

To check our contention that there should not exist a unique relation between extinction and LWC in fog, regardless of the form of the droplet size distribution or value of the wavelength, we compare empirical relationships between extinction at visible wavelengths and LWC determined by other workers for fog measurements made under different meteorological conditions and at different geographical locales. For the present work we can derive the following approximate empirical relation between extinction at 0.55 μm and LWC from the results in Fig. 10a:

$$\beta_{ext}(0.55) \approx 145 w^{0.63}, \tag{2}$$

where $\beta_{ext}(0.55)$ refers to the particulate extinction coefficient (km^{-1}) at 0.55 μm and w refers to liquid water content (g m^{-3}). For comparison Eldridge (1971) gives the empirical relation

$$\beta_{ext}(0.55) \approx 160 w^{0.65}, \tag{3}$$

for fogs and hazes having liquid water content 0.001–0.2 g m^{-3}. For fogs in the Tsei gorge near Leningrad with liquid water content 0.0002–0.2 g m^{-3}, Barteneva and Polyakova (1965) find

$$\beta_{ext}(\text{visible}) \approx 142 w^{0.87}. \tag{4}$$

From Kumai's (1973) simultaneous measurements of arctic fog size distribution and prevailing visual range at Point Barrow, AK, with liquid water content 0.005–0.1 g m^{-3}, we find

$$\beta_{ext}(\text{visible}) \approx (100\text{–}200) w, \tag{5}$$

where the extinction has been inferred from the visual range measurements using Koschmieder's relation for a threshold ratio of 2%. Kumai has calculated the extinction from the measured size distributions as we have done and the visual range calculated from these extinction values at 0.55 μm are in good agreement with his measurements of visual range.

Using these four empirical expressions relating visible extinction to LWC, for an LWC of 0.01 g m^{-3}, we get extinction coefficients of 8.0, 8.0, 2.6 and 1.0–2.0 km^{-1}, respectively, for the present work, Eldridge, Barteneva and Polyakova, and Kumai. These values differ by roughly an order of magnitude. These differences are most likely due to the widely differing fog droplet size distributions measured by the various authors, and thus any size-distribution-independent relation between extinction (at visible wavelengths) and LWC cannot be applied to fogs in general.

The approximation proposed by Chýlek (1978) can also be used to explain the approximate $1/\lambda$ wavelength dependence of extinction for haze evident in Figs. 9a and 9b. The approximation can be written in the form

$$\beta_{ext}(\lambda) \approx \frac{3\pi c}{2\rho\lambda} w, \tag{6}$$

where w is the liquid water content, ρ the density of water and the coefficient c is equal to the slope of a

straight line approximating the efficiency factor for extinction by

$$Q_{\text{ext}}(x,\lambda)\approx c(\lambda)x. \tag{7}$$

The coefficient c is a slowly varying function of wavelength. For two wavelengths λ_1, λ_2 the approximation (6) can be rewritten

$$\beta_{\text{ext}}(\lambda_1)\approx\frac{c_1\lambda_2}{c_2\lambda_1}\beta_{\text{ext}}(\lambda_2), \tag{8}$$

relating extinction at one wavelength to that at another. This approximation is only valid for polydispersions of droplets having a size parameter less than a maximum value x_m, or equivalently, a maximum radius r_m. From Chýlek's (1978) Table 1 the maximum radii and corresponding c values are at $\lambda=0.5$ μm, $r_m=0.5$ μm, $c=0.61$; at $\lambda=3.8$ μm, $r_m=3.6$ μm, $c=0.68$; and at $\lambda=10$ μm, $r_m=12$ μm, $c=0.35$. Haze particles have maximum radii of about 2 μm (Figs. 6a and 6b); hence the approximation (8) can be applied at 4 and 10 μm wavelengths and we obtain β_{ext} (4 μm)$\approx$4.9 β_{ext} (10 μm), in good agreement with the exact Mie results in Figs. 9a and 9b. At the 0.55 μm wavelength the Chýlek approximation cannot legitimately be used since particles with radii greater than the maximum value ($r_m\approx0.5$ μm) contribute a significant part of the extinction for some haze distributions. Nevertheless, if we apply the approximation we obtain β_{ext} (0.55 μm) $\approx6.5\,\beta_{\text{ext}}$ (4 μm), a result that is within a factor 2 of the exact Mie results in Figs. 9a and 9b.

6. Conclusions

Measurements of haze and fog droplet distributions carried out during eight days in wintertime in West Germany show little vertical structure for haze, but a general trend toward increasing concentration of 4–16 μm radius droplets with altitude for fog conditions with visibilities <1 km. Particulate extinction calculated from measured distributions at 0.55, 4 and 10 μm wavelengths shows increases by a factor of 2 to 1000 over the first 150 m altitude for fog. Extinction is found to be approximately proportional to $1/\lambda$ over this spectral region for haze conditions, but nearly independent of wavelength for fog. There exists a size-distribution-independent linear relationship between particle extinction coefficient and liquid water content at 10 μm. However, the approximate relationships found between extinction (from visible through 4 μm wavelengths) and liquid water content is attributed to a common form of the fog and haze size distributions measured.

Acknowledgments. We acknowledge Mr. Lucien Biberman of the Institute for Defense Analysis for his suggestion that we look into the correlation of extinction in the infrared and liquid water content. Upon request the authors will send to interested workers a more complete technical report of this work.

REFERENCES

Arnulf, A., J. Bricard, E. Cure and C. Veret, 1957: Transmission by haze and fog in the spectral region 0.35 to 10 microns. *J. Opt. Soc. Amer.*, **47**, 491–498.

Barteneva, O. D., and E. A. Polyakova, 1965: A study of attenuation and scattering of light in a natural fog due to its microphysical properties. *Izv. Atmos. Oceanic Phys.*, **1**, 193–207.

Chýlek, Petr, 1978: Extinction and liquid water content of fogs. *J. Atmos. Sci.*, **35**, 296–300.

Eldridge, R. G., 1961: A few fog drop-size distributions. *J. Appl. Meteor.*, **18**, 671–676.

——, 1966: Haze and fog aerosol distributions. *J. Atmos. Sci.*, **23**, 605–613.

——, 1971: The relationship between visibility and liquid water content in fog. *J. Atmos. Sci.*, **28**, 1183–1186.

Garland, J. A., 1971: Some fog droplet size distributions obtained by an impaction method. *Quart. J. Roy. Meteor. Soc.*, **97**, 483–494.

——, J. R. Branson and I. C. Cox, 1973: A study of the contribution of pollution to visibility in a radiation fog. *Atmos. Environ.*, **7**, 1079–1092.

Goodman, J., 1977: The microstructure of California coastal fog and stratus. *J. Appl. Meteor.*, **16**, 1056–1067.

Hale, G. M., and M. R. Querry, 1973: Optical constants of water in the 200 nm to 200 μm wavelength region. *Appl. Opt.*, **12**, 555–563.

Hänel, G., 1971: New results concerning the dependence of visibility on relative humidity and their significance in a model for visibility forecast. *Beitr. Phys. Atmos.*, **44**, 137–167.

Krasikov, P. N., and G. A. Chikirova, 1956: Microphysical characteristics of local fogs. *Tr. Gl. Geofiz. Observ.*, **57**, 88–100.

Kumai, M., 1973: Arctic fog droplet size distribution and its effect on light attenuation. *J. Atmos. Sci.*, **30**, 635–643.

Kunkel, B. A., 1971: Fog drop-size distributions measured with a laser hologram camera. *J. Appl. Meteor.*, **10**, 482–486.

Laktionov, A. G., 1967: Variation of the size and concentration of drops during the scattering of fog. *Izv. Atmos. Oceanic Phys.*, **3**, 566–569.

Low, R. D. H., 1975: Microphysical evolution of fog. *J. Rech. Atmos.*, **2**, 23–32.

May, K. R., 1961: Fog droplet sampling using a modified impactor technique. *Quart. J. Roy. Meteor. Soc.*, **87**, 535–548.

Patterson, E. M., 1977: Atmospheric extinction between 0.55 and 10.6 μm due to soil-derived aerosols. *Appl. Opt.*, **16**, 2414–2418.

Pilié R. J., E. J. Mack, W. C. Kocmond, W. J. Eadie and C. W. Rogers, 1975: The life cycle of valley fog. Part II: Fog microphysics. *J. Appl. Meteor.*, **14**, 364–374.

Pinnick, R. G., J. M. Rosen and D. J. Hofmann, 1973: Measured light-scattering properties of individual aerosol particles compared to Mie scattering theory. *Appl. Opt.*, **12**, 37–41.

Roach, W. T., R. Brown, S. J. Caughly, J. A. Garland and C. J. Readings, 1976: The physics of radiation fog: I—a field study. *Quart. J. Roy. Meteor. Soc.*, **102**, 313–333.

Rosen, J. M., 1968: Simultaneous dust and ozone soundings over North and Central America. *J. Geophys. Res.*, **73**, 479–486.